Sains Malaysiana 54(6)(2025): 1535-1549
http://doi.org/10.17576/jsm-2025-5406-09

Synthesis and Characterization of 5,15 A_{2}-Type Porphyrin, Metalloporphyrin and Preliminary Study on Carbon Dioxide Adsorption

(Sintesis dan Pencirian Porfirin Jenis 5,15 A_2, Metaloporfirin dan Kajian Awal tentang Penjerapan Karbon Dioksida)

NUUR HAZIQAH MOHD RADZUAN[1], ZAITUN GHAZALI[1], NURUL IZZATY HASSAN[1], MOHD BAKRI BAKAR[2], SITI AISHAH HASBULLAH[1] & MUNTAZ ABU BAKAR[1,*]

[1]Department of Chemical Sciences, Faculty of Science & Technology, Universiti Kebangsaan Malaysia, 43600 UKM Bangi, Selangor, Malaysia
[2]Department of Chemistry, Faculty of Science, Universiti Teknologi Malaysia, 84600 Pagoh, Johor, Malaysia

Received: 9 January 2025/Accepted: 26 April 2025

ABSTRACT

Porphyrins are among the most extensively studied compounds in chemistry due to their remarkable stability, optical, and photophysical properties. In recent years, advancements in their diverse applications have driven the exploration of porphyrins with different functional groups, allowing for more specific applications. Nowadays, a greater focus is being placed on the development of materials for capturing and converting carbon dioxide (CO_2) into value-added products. Despite their promising features, the application of porphyrins in carbon dioxide adsorption has been hindered by their initially low adsorption capacity compared to other traditional porous materials, such as microporous carbons and zeolites. Modifications to porphyrins, such as the introduction of diverse functional groups and the incorporation of metal centers are promising, as they may enhance the CO_2 adsorption performance of porphyrin-based materials. Therefore, this study focuses on the synthesis of 5,15 A_2-type porphyrin and its metalloporphyrin derivatives, along with a preliminary evaluation of synthesized porphyrin's carbon dioxide adsorption ability. The synthesized porphyrins were characterized via nuclear magnetic resonance spectroscopy (NMR) and UV-visible spectroscopy. The yield for porphyrin varied from 23% to 35%, while metalloporphyrin achieved a yield of 99%. A preliminary study of carbon dioxide adsorption ability of porphyrin and metalloporphyrin showed that the insertion of metal into the center of porphyrin macrocyclic ring enhances the binding affinity and improves adsorption capacity. The Freundlich isotherm showed the presence of heterogeneous adsorption sites and possible multilayer adsorption of CO_2 onto the porphyrin's surface. Additionally, due to the ability of metalloporphyrin to adsorb CO_2, metalloporphyrin has the potential to serve as a building block for the integration of porphyrin into hybrid materials such as metal-organic frameworks (MOFs) and covalent-organic framework (COFs), by enhancing their structural stability and CO_2 performance.

Keywords: Carbon dioxide adsorption; covalent-organic frameworks (COFs); metalloporphyrin; metal-organic frameworks (MOFs); 5,15-A_2-porphyrin

ABSTRAK

Porfirin merupakan antara sebatian yang paling banyak dikaji dalam bidang kimia kerana kestabilannya yang luar biasa serta sifat optik dan fotofizikal yang menonjol. Dalam beberapa tahun kebelakangan ini, kemajuan dalam pelbagai aplikasi telah mendorong penerokaan porfirin dengan kumpulan berfungsi yang berbeza, kerana perbezaan ini boleh membawa kepada aplikasi khusus yang berlainan. Pada masa kini, tumpuan yang lebih besar diberikan kepada pembangunan bahan untuk menangkap dan menukar karbon dioksida kepada produk yang mempunyai nilai tambah. Walaupun porfirin berpotensi sebagai bahan penjerap disebabkan ciri yang dimiliki, penggunaannya dalam penjerapan karbon dioksida masih terhad disebabkan kapasiti penjerapan yang rendah pada peringkat awal berbanding dengan bahan yang mempunyai kadar liang yang tinggi seperti karbon mikropori dan zeolit. Bagi mengatasi kekangan ini, pengubahsuaian terhadap struktur porfirin seperti memperkenalkan kumpulan berfungsi yang pelbagai dan menyepadukan pusat logam perlu diberi penekanan. Hal ini kerana pengubahsuaian ini berpotensi meningkatkan prestasi penjerapan karbon dioksida bagi bahan berasaskan porfirin. Oleh itu, kajian ini memberi tumpuan kepada sintesis porfirin jenis A_2-5,15, terbitan metaloporfirin dan penilaian awal terhadap keupayaan penjerapan karbon dioksida. Porfirin yang disintesis telah dicirikan menggunakan Spektroskopi NMR dan Spektroskopi UV-Vis. Hasil perolehan porfirin adalah antara 23% hingga 35%, manakala metaloporfirin mencapai hasil sebanyak 99%. Kajian awal terhadap penjerapan karbon dioksida bagi porfirin A_2-5,15 dan metaloporfirin menunjukkan bahawa penyepaduan pusat logam meningkatkan keupayaan pengikatan karbon dioksida dan menambah baik kapasiti penjerapan. Model isoterma Freundlich menunjukkan kehadiran tapak penjerapan heterogen dan kemungkinan berlakunya penjerapan berbilang lapisan karbon dioksida pada permukaan porfirin. Selain itu, disebabkan kebolehan metaloporfirin untuk menjerap karbon dioksida, metaloporfirin berpotensi untuk digunakan sebagai blok binaan untuk menghasilkan bahan hibrid seperti rangka logam-organik (MOF) dan rangka organik-kovalen (COF) bagi meningkatkan kestabilan struktur dan kecekapan penjerapan karbon dioksida.

Kata kunci: Metaloporfirin; penjerapan karbon dioksida; rangka logam-organik (MOF); rangka organik-kovalen (COF); 5,15-A_2-porfirin

INTRODUCTION

Porphyrin has attracted the interest of scientists worldwide because of its unique characteristics, which offer a wide range of potential applications. Porphyrin has been applied as a photosensitizer in photodynamic treatment (PDT), an artificial photosynthesis system, and a catalyst for carbon dioxide conversion. Porphyrins are nature's preferred catalysts due to their unique characteristics and robust structure (Kumar et al. 2015). Carbon dioxide (CO_2) is essential to the ecosystem as it helps to maintain the equilibrium of the planet's temperature and atmosphere. However, global warming, rising sea levels, and ocean acidification are primarily driven by anthropogenic carbon dioxide which is the dominant greenhouse gas (Kumar et al. 2015). According to recent data, global energy-related carbon dioxide emissions have continued to rise over the past decade. In 2022, emissions reached approximately 36.8 gigatons (Gt), marking a 0.9% increase from the previous year (IEO 2022). This upward trend persisted into 2023, with emissions growing by an additional 1.1%, to a new record high of 37.4 Gt (IEO 2023).

Based on the growing concern about higher levels of carbon dioxide gas, researchers are working on the development of systems that are capable of adsorbing or capturing carbon dioxide and converting it into value-added products. Solid adsorbents are among the most promising candidates for application in CO_2 capture technologies (Creamer & Gao 2015). Solid adsorbents such as zeolites, activated carbon, carbon nanotubes, and silicon-based materials have been extensively studied for CO_2 capture. These materials are typically characterized in terms of their surface functional groups, porosity, surface area, pore size distribution, metal coordination sites, and electrostatic interactions to evaluate their potential as effective CO_2 adsorbents (Creamer & Gao 2015). Consequently, porphyrins are consistently promising in providing these benefits (Kumar et al. 2015). Porphyrins, as organic solid adsorbents, are promising for low-temperature CO_2 adsorption due to their surface properties, particularly their high surface area, which enables further modification through the incorporation of additional metal centers and functional groups. The adsorption of gases onto solid surface arises from physical adsorption which is mainly controlled by van der Waals forces between the surface of the adsorbent and adsorbate molecules. Another mechanism of adsorption is chemical adsorption or chemisorption, in which where the surface of adsorbent interacts with adsorbate molecules through weak chemical bonds (Creamer & Gao 2015). However, porphyrin, and especially free-base porphyrin, has often been regarded offering poor adsorption compared to zeolites and microporous carbon due to its inherently planar structure, which results in low surface area and limited porosity. This has been addressed by introducing new insights, particularly the structural enhancement of porphyrins via the incorporation of diverse functional groups and metal centres into the porphyrin ring. These modifications can improve surface area and pore volume, thereby enhancing CO_2 adsorption capacity. In recent years, numerous studies have utilized porphyrins as building blocks for the development of hybrid adsorbent materials, such as metal–organic frameworks (MOFs), owing to their unique macrocyclic structure. Porphyrins can be readily integrated into organic frameworks by forming interlinks with rigid units, which leads to the formation of porous organic polymers (Kumar et al. 2015). The CO_2 adsorption performance of porphyrins with various functional groups incorporated into MOFs has been reported by Rajasree, Li and Deria (2021), who emphasized that different functional groups significantly influence the adsorption efficiency of the resulting frameworks. Similarly, Liu et al. (2013) developed a copper (II) porphyrin-based MOF exhibiting enhanced CO_2 capture and photoreduction capabilities. The presence of Cu (II) centres and conjugated porphyrin ligands promoted strong interactions with CO_2, resulting in significantly improved uptake compared to conventional physisorptive materials. Hence, the electronic properties of porphyrins can be precisely tuned by modifying the peripheral functional groups and altering the identity of the central metal.

Additionally, axial coordination plays a crucial role in shaping both the electronic structure and functional performance of the material (Rajasree, Li & Deria 2021). Given that copper-based porphyrins have shown considerable promise in CO_2 adsorption and are commonly used in MOFs integration, this study aims to broaden the scope by synthesizing and evaluating zinc- and nickel-based porphyrins as potential CO_2 adsorbents. Furthermore, there are limited reported studies evaluating CO_2 adsorption ability of A_2-type porphyrin compared to the more studied A_4-type porphyrin. A_2-type porphyrin refers to a porphyrin molecule bearing two identical functional groups at two meso positions, whereas A_4-type porphyrin contains four identical functional groups at all four meso positions of the macrocyclic ring, and is generally more straightforward to synthesize. Unlike A_4-type porphyrin, A_2-type porphyrin offers asymmetric substitution patterns that allow for more flexible functionalization (Senge et al. 2015). Hence, in this study, 5,15-A_2-porphyrins with hexyl and phenyl functional groups together with metalloporphyrins derivatives were synthesized, and preliminary evaluation on carbon dioxide adsorption ability of porphyrins and metalloporphyrins were conducted by evaluating the physical adsorption of carbon dioxide gas molecule onto the surface of porphyrin compound.

RESULTS AND DISCUSSION

SYNTHESIS

Dipyrromethane

The synthetic path to porphyrin derivatives began with the synthesis of dipyrromethane. Dipyrromethane plays an important role in porphyrin chemistry as the building block of porphyrin compound (Pereira & Pinho 2014). Since 1994, several dipyrromethene synthesis route have been developed, including a trifluoroacetic acid-catalyzed condensation reaction between pyrrole and paraformaldehyde (Figure 1(a)). This reaction requires the elimination of excess pyrrole, followed by purification via Kugelrohr distillation (Laha et al. 2003; Pereira & Pinho 2014; Shanmugathasan, Edwards & Boyle 2000). The purpose of this distillation process is to eliminate the higher oligomers formed by this reaction.

5,15- A_2porphyrins

5,15-A_2 porphyrin was synthesized by [2+2] condensation process between the building block dipyrromethane and different aldehydes, including benzaldehyde and heptanal (Figure 1(b)). In this reaction, pair of carbon bridges connected two dipyrromethanes, and substituents were inserted at two carbon locations. The condensation reaction creates an intermediate molecule known as porphyrinogen, which when oxidized by an oxidizing agent yielded 5,15-A_2 porphyrin as a result of porphyrinogen conversion. Trifluoroacetic acid (TFA) is commonly used as a catalyst in aldehyde condensation reactions due to its highly-electronegative fluorine atom and the electron-withdrawing characteristic of trifluoromethyl weaken the oxygen-hydrogen bond, increasing the acidity of the catalyst. The protonation process of oxygen in the aldehyde group is facilitated by the catalyst's higher acidity.

METALLATION OF PORPHYRINS

The metallation of free-base porphyrin with zinc is carried out in chloroform in the presence of excess zinc (II) acetate (Figure 1(c)). Zinc (II) typically forms porphyrin complexes rapidly at room temperature. Therefore, chloroform, with its boiling point of 61 °C, is preferred as the solvent, as it provides suitable conditions for the metallation reaction under mild conditions. In contrast, the metallation of porphyrin with nickel (II) acetylacetonate is typically conducted at high temperatures using a nonpolar or weakly polar solvent such as toluene. This solvent choice is necessary due to the strong coordination complexes formed between nickel (II) and porphyrins, which require elevated temperatures to drive the reaction to completion. Toluene, with its high boiling point (~110 °C), allows the reaction to proceed efficiently at high temperatures without excessive solvent evaporation. Both chloroform and toluene are non-coordinating solvents, making them suitable for the metallation of porphyrins, as they do not interfere with the metal insertion process.

NMR STUDIES

All ^{1}H NMR spectra were recorded at room temperature in deuterated chloroform. Figure 2 illustrates the NMR spectrum of porphyrin building block dipyrromethane **1**. Due to the similar environment of dipyrromethane's symmetrical structure, the location of protons is symmetrical, resulting in five chemical shift signals indicating ten hydrogens in dipyrromethane. A broad singlet peak at 7.70 ppm corresponds to two protons of NH secondary amine groups. This proton exhibits a low-field chemical shift because of the high electronegative nitrogen atom connected. At 6.64 and 6.22 ppm, there are two quartet and doublet peaks, representing two protons for each peak. The chemical shift at 3.97 ppm corresponds to two protons from the methylene group (CH_2) that joins two pyrrole molecules. All of the chemical shift values for dipyrromethane obtained agree with the findings reported by Basic (2010).

The spectrum in Figure 3(a) shows that 5,15-A_2 porphyrin **2** displays six chemical shift peaks, which correspond to a total of 20 protons. The appearance of a peak in the high-field region with a negative chemical shift value indicates the successful formation of porphyrin **2** and other free-base porphyrins. The chemical shift around -3 ppm suggested the existence of an amine group proton (NH) in the center of porphyrin macrocyclic ring. These protons are highly shielded due to the anisotropic effect created by the porphyrin ring π-electron system. In the porphyrin's structure, protons located outside the ring experience deshielding, leading to a downfield chemical shift. In contrast, protons situated in the centre of the macrocycle, such as the NH protons, are oriented differently with respect to the anisotropic field, resulting in strong shielding and a negative chemical shift. Hence, the chemical shift of the proton on the phenyl group's carbon at the meso position appears at the most deshielded region, at around 10 ppm.

Upon metallation, the central NH protons are replaced, and the overall electronic distribution in the macrocycle changes. This typically eliminates the negative chemical shift as metal coordination alters the electronic environment, reducing the shielding effect. This can be seen in Figure 3(b) and 3(c), which shows no negative chemical shift when the inner porphyrin proton is replaced by metal ion. Additionally, Ni (II) porphyrin exhibits greater

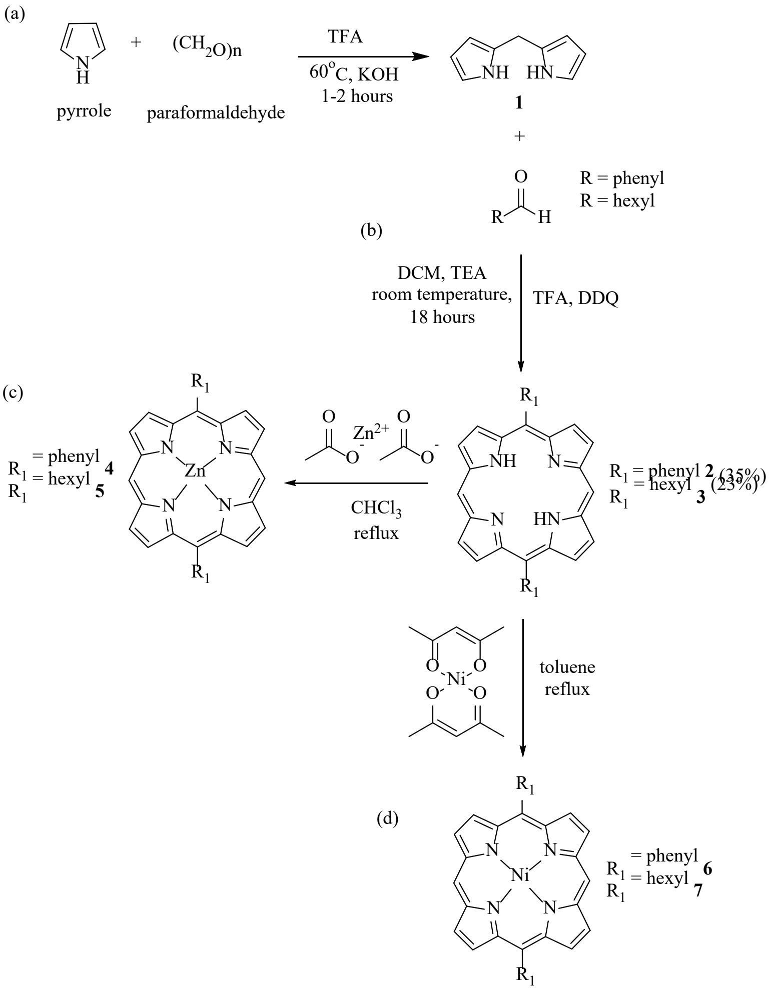

FIGURE 1. Reaction scheme (a) synthesis of dipyrromethane, (b) synthesis of 5,15-A_2 porphyrin, (c) metallation of porphyrins with zinc (II), and (d) metallation of porphyrins with nickel (II)

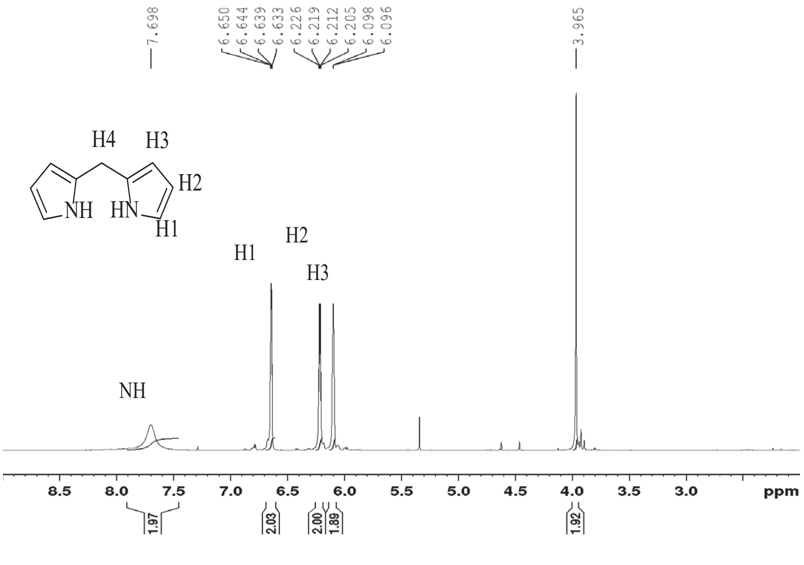

FIGURE 2. NMR spectrum of dipyrromethane **1** in $CDCl_3$ at room temperature

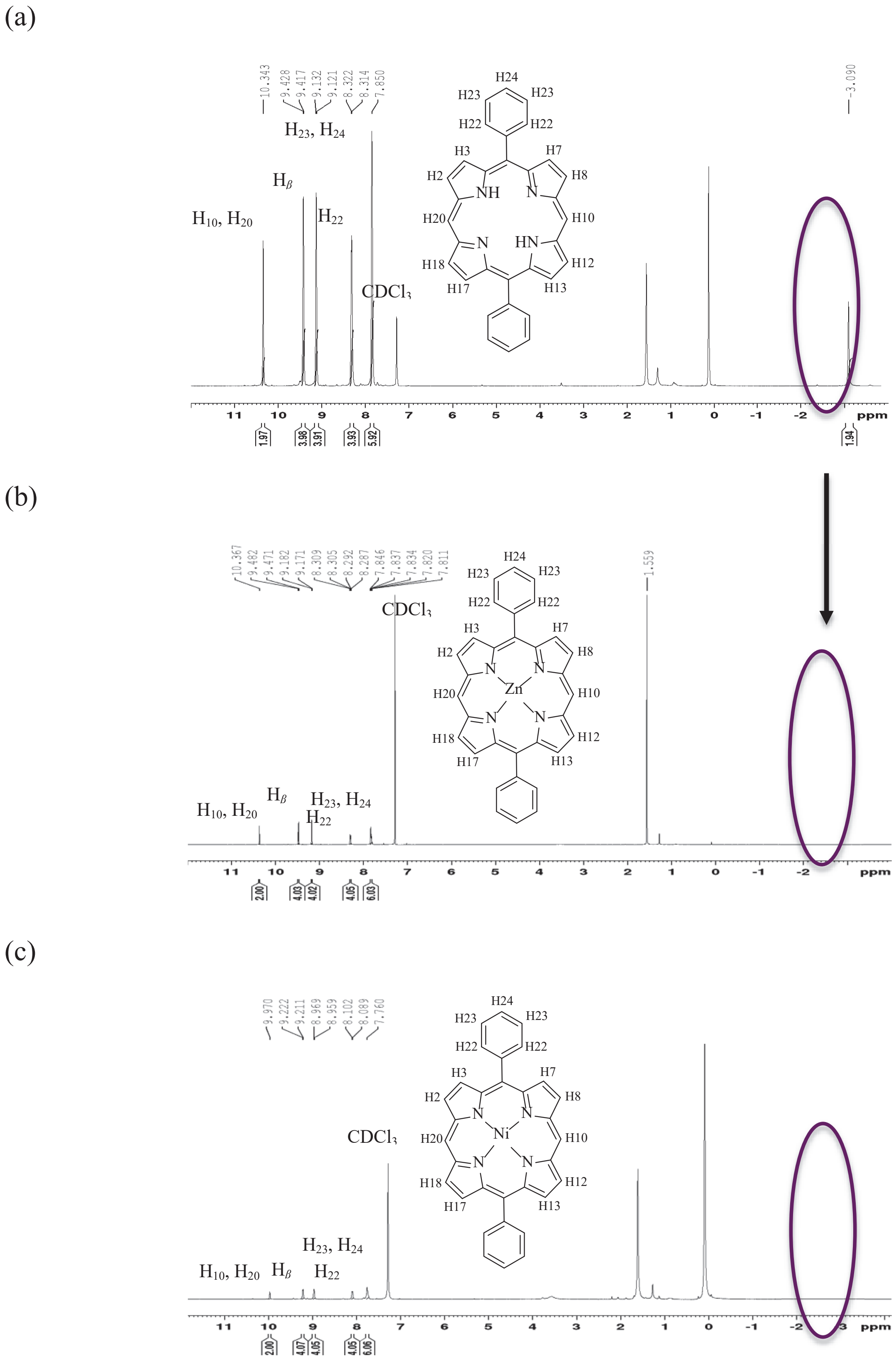

FIGURE 3. NMR spectrum of porphyrin (a) **2**, (b) **4**, and (c) **6** in $CDCl_3$ at room temperature

shielding effects in ^{1}H NMR spectroscopy as compared to Zn (II) porphyrin due to its rigid square-planar coordination geometry which enhance π-electron delocalization across the macrocycle. Unlike zinc (II) porphyrin, which adopts a tetrahedral coordination environment and often binds axial ligands, nickel (II) porphyrin remains strictly planar, preserving electron delocalization and increasing shielding effects. The shielding effect of Ni (II) porphyrin as compared to Zn (II) porphyrin can be seen based on the chemical shift signal or meso and β protons in Figure 3(b) and 3(c). The 5,15-A_2 porphyrin **3** with hexyl functional groups at two meso positions exhibits the similar H-NMR behavior (Spectrum available in the supplementary data).

UV-VISIBLE SPECTROSCOPY STUDY

Ultraviolet-visible (UV-Vis) spectroscopy is a fascinating technique used to characterize porphyrin. This is due to the physical color preference of individual porphyrin, which is the result of porphyrin's high absorption rate in the visible part of the electromagnetic spectrum. The porphyrin compound shows spectrum within the wavelength range of 350 to 800 nm. This high-intensity signal, known as the Soret band, can be observed within the wavelength range of 400 to 450 nm whereas the Q band appears in the wavelength range of 500 to 650 nm. Gouterman's four-orbital model, as described by Wamser and Ghosh (2022), provides an explanation for the formation of Soret and Q bands that arise from π-π* transitions. Figure 4 depicts Gouterman's four-orbital model, including two π orbitals (a_{1u} and a_{2u}) and a degenerate π* orbital (e_{gx} and e_{gy}).

The two highest occupied molecular orbitals (HOMO) on the π bond, which have identical energy levels, generate a strong configurational interaction between the a_{1u} to e_g and a_{2u} to e_g transitions (Shi, Zhang & Linhardt 2021). The phenomenon of constructive interference results in the high intensity of the Soret band, which corresponds to a strong π- π* transition from S_0 to S_2 (Figure 4), whereas the Q band arises from lower energy of π- π* transition from S_0 to S_1 and exhibits a lower intensity due to destructive combinations (Wamser & Ghosh 2022). Additionally, the difference in intensity between these bands is due to the extent of orbital mixing, with the Soret band being significantly more intense than the Q bands due to stronger transition dipole interactions. Characterizations of free-base porphyrin and metal porphyrin can be differentiated via the number of Q bands that appear. Free-base porphyrin (D_2h symmetry) exhibits four Q bands, namely $Q_x(0,0)$, $Q_y(0,0)$, $Q_x(1,0)$, and $Q_y(1,0)$ due to NH induced energy splitting. The metallation of porphyrin removes NH groups and restores D_4h symmetry. Thus, the Q bands will be reduced to two which Q(0,0) and Q(1,0) and sometimes only one Q band can be seen. The number of Q bands decreases upon metallation due to increase of symmetry, eliminated the NH-based perturbations. Figure 5 showed the example of UV-Visible spectrum of free-base and metalloporphyrin obtained from previous reported data whereas Figure 6 illustrated the UV-Visible spectrum of free-base porphyrin **2**, which showed the existence of one Soret band and four Q bands, whereas metalloporphyrins **4** and **6** have only one Soret band and two Q bands.

PRELIMINARY EVALUATION ON CARBON DIOXIDE ADSORPTION ABILITY

A preliminary study was carried out to determine the carbon dioxide adsorption ability of porphyrin and assess its potential for adsorbing carbon dioxide gas. The carbon dioxide adsorption of free-base 5,15-A_2 porphyrin with different substituent groups, specifically 5,15-diphenylporphyrin **2** and 5,15-dihexylporphyrin **3**, was evaluated. In addition, the carbon dioxide adsorption capacities of Zn (II) porphyrin **4** and **5**, as well as Ni (II) porphyrin **6** and **7**, were also assessed using a gas adsorption analyzer. This instrument requires a degassing process for six to ten hours to remove any moisture content in the compound that might affect the surface interaction of the compound with carbon dioxide gas molecules. The carbon dioxide adsorption rate by porphyrin is quantified by assessing the extent of interaction between the compound's surface and pores with carbon dioxide gas molecules. Table 1 presents the carbon dioxide adsorption capacity for each porphyrin, while Figure 7 displays the carbon dioxide gas adsorption isotherm for six analyzed porphyrin compounds.

CO_2 uptake is primarily governed by the availability of accessible micropores, a highly exposed surface area, and a large pore volume (Ghazali et al. 2020). As for porphyrin, the physical adsorption of CO_2 onto porphyrin occurs through weak, non-covalent interaction. This process is primarily influenced by the porphyrin's surface properties, metal center interactions and π-electron systems. CO_2 is a linear, non-polar molecule with quadrupole moment which enables it to engage in weak dispersion forces with porphyrin surface. Porphyrins with extended π-conjugation systems can enhance these interactions through π–quadrupole attractions, facilitating physical adsorption. Additionally, CO_2 exhibits a partial negative charge on the oxygen atoms and a partial positive charge on the central carbon atom. Porphyrins, especially those with polarizable electron clouds, can interact with CO_2 through electrostatic attraction, further contributing to physical adsorption. The carbon dioxide adsorption isotherm depicted in Figure 7 demonstrates that Zn (II) porphyrins with phenyl and hexyl substituents have a higher rate of carbon dioxide adsorption compared to both free-base and Ni (II) porphyrins. Metalloporphyrin can lead to weak axial coordination to CO_2, especially if the metal center has an open site such as zinc. Conversely, Ni (II) porphyrins have a rigid square-planar structure, which restricts the accessibility of axial coordination sites and limits surface interactions with CO_2 molecules. In contrast, free-base porphyrins, which lack a central metal, rely primarily on π-electron

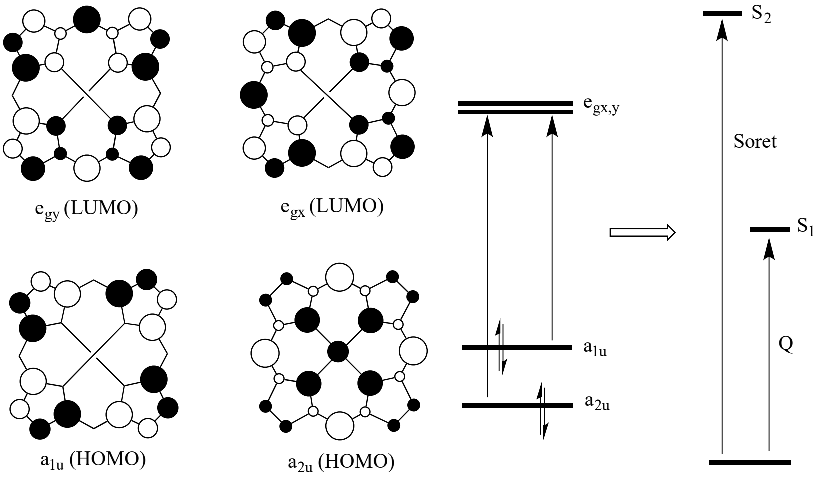

Source: Giovannetti (2012)

FIGURE 4. Gouterman's four-orbital model

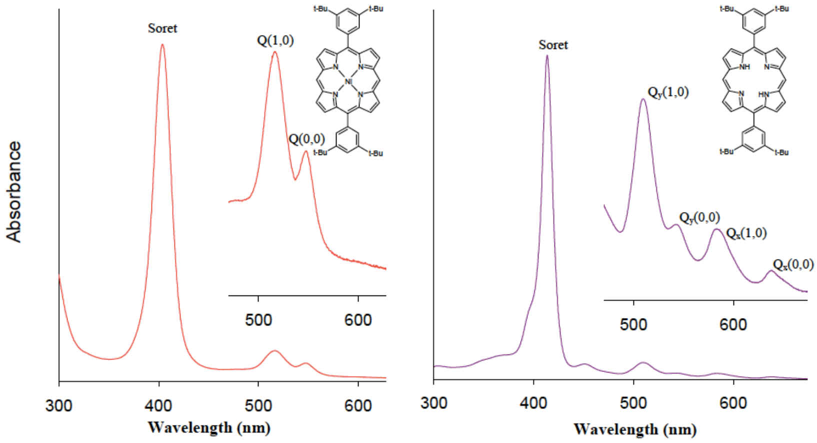

Source: Locos (2006)

FIGURE 5. Example of UV Vis spectrums of free-base porphyrin and metalloporphyrin

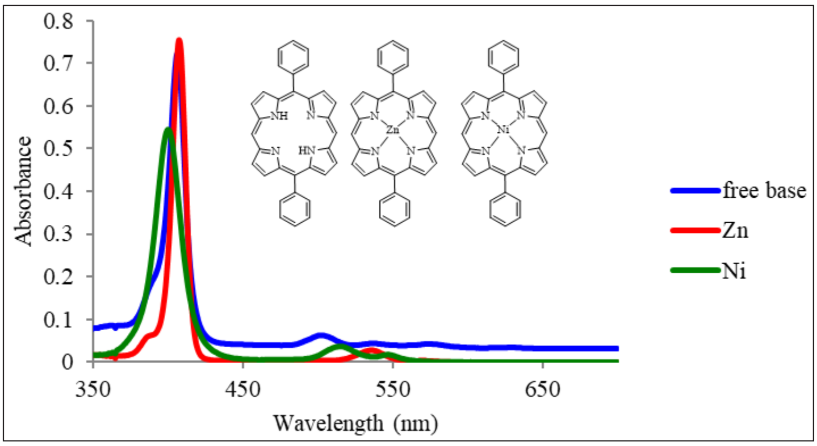

FIGURE 6. UV-Visible spectrum of free-base porphyrin **2** and metalloporphyrin **4** and **6** at concentration of 1.0×10^{-6} M in dichloromethane ($CHCl_2$) at room temperature

TABLE 1. Data of carbon dioxide gas adsorption

Porphyrin compound	Carbon dioxide gas adsorption at 25 °C (cm^3/g)	Adsorption capacity at 25 °C (mg CO_2/g adsorbent)
5,15 –diphenylporphyrin **2**	4.10	8.05
Zn-5,15-diphenylporphyrin **4**	31.65	62.16
Ni-5,15-diphenylporphyrin **6**	18.78	36.88
5,15-dihexylporphyrin **3**	30.85	60.59
Zn-5,15-dihexylporphyrin **5**	50.41	99.01
Ni-5,15-dihexylporphyrin **7**	22.70	44.58

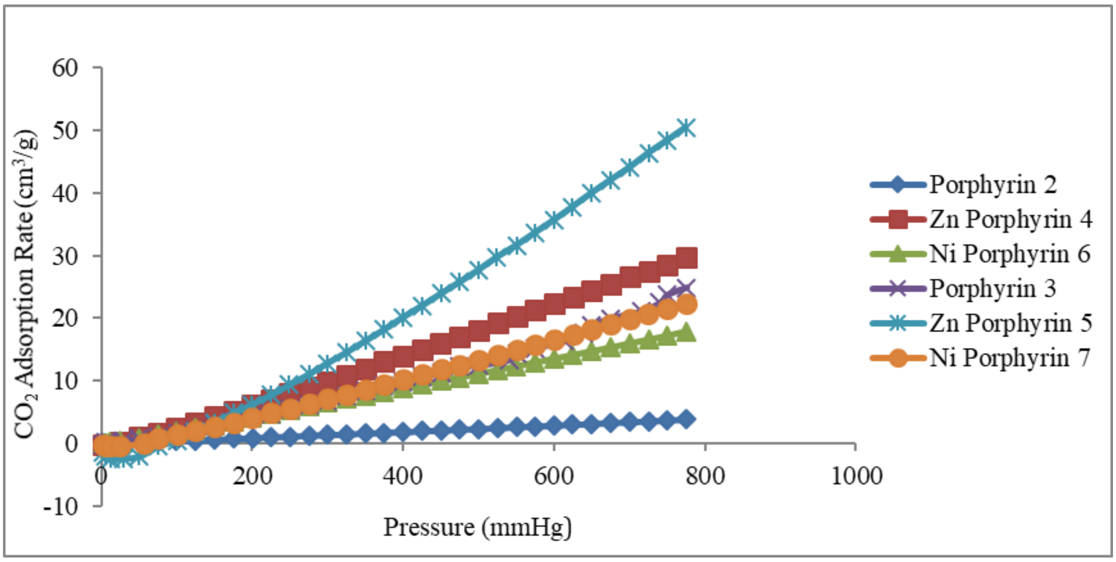

FIGURE 7. Carbon dioxide adsorption isotherm at temperature of 25 °C

interactions and surface effects for CO_2 adsorption. Additionally, Zn is more electropositive enhancing CO_2 polarization and attraction. Based on Table 1, the CO_2 uptake ability of Zn (II) porphyrin with hexyl substituent is higher compared to the Zn (II) porphyrin with phenyl substituent. This phenomenon could be due to several structural and electronic factors. The flexible, aliphatic nature of hexyl chains promotes looser molecular packing, resulting in increased porosity and greater accessible surface area for CO_2 diffusion and adsorption. In contrast, phenyl substituents are bulky and rigid, often leading to tighter packing and significant π–π stacking interactions, which reduce the available free volume and limit access to the active sites. Furthermore, the steric hindrance imposed by phenyl rings can partially block the axial coordination site of the central Zn^{2+} ion, thereby decreasing its ability to interact with CO_2. Figure 8 illustrates the adsorption and desorption isotherm of Zn-porphyrin **5**, which exhibits the highest rate of CO_2 adsorption among the compounds tested.

The adsorption desorption isotherm of Zn-porphyrin **5** in Figure 8 indicates that the desorption of this compound is irreversible, stopping at pressure of 50 mmHg and forming an unclosed loop. Liu et al. (2013) discovered that the occurrence of open adsorption and desorption isotherm phenomena suggests a favorable chemisorption of CO_2 on porphyrin compounds. This result demonstrates that CO_2 is not just physically adsorbed to the surface of porphyrin, but might also chemically bonded to the porphyrin. While physisorption is governed by weak van der Waals forces or electrostatic interactions, chemisorption involves the formation of strong covalent or ionic bonds between the adsorbate (CO_2) and specific active sites on the adsorbent. This implies that the porphyrin surface, particularly in the presence of a metal center, may provide reactive sites capable of forming stronger and more permanent interactions with CO_2 molecules.

Additionally, the adsorption data for Zn-porphyrin **5** was further analyzed using the Langmuir and Freundlich isotherm models. The Langmuir isotherm assumes that

CO_2 uptake occurs on a homogeneous surface through monolayer adsorption, as described by Marliza et al. (2017). The Langmuir equation can be expressed in the following linear form:

$$P/Q = (1/Q_o b) + (P/Q_o) \text{ (Marliza et al. 2017)} \qquad (1)$$

where P is the equilibrium pressure (mmHg); Q is the amount of CO_2 adsorbed at equilibrium (mg/g); Q_o is the maximum monolayer adsorption capacity (mg/g); b is the Langmuir constant.

The values of Q_o and b can be determined from the slope and intercept of Langmuir equation. The Freundlich isotherm model is used to describe the adsorption characteristic for the heterogenous surface. The linear equation for this isotherm is as follows:

$$\log Q = 1/n \log P + \log K_f \text{ (Marliza et al. 2017)} \qquad (2)$$

where P is the equilibrium pressure (mmHg); Q is the amount of CO_2 adsorbed at equilibrium; K_f is the indicator for adsorption capacity; 1/*n* is the function of the adsorption strength in the adsorption process.

The experimental CO_2 adsorption data did not exhibit a good linear correlation in the Langmuir isotherm plot, indicating that the adsorption process does not follow ideal monolayer behavior. This deviation suggests the presence of heterogeneous adsorption sites and possible multilayer adsorption. In contrast, the Freundlich isotherm model produced a linear equation with a correlation coefficient R^2= 0.984, indicating a good fit to the experimental data. The model yielded a K_f value of 0.00151 and 1/*n* value of 0.595, which is suggesting favorable adsorption on a heterogeneous surface. A smaller 1/*n* value typically indicates greater surface heterogeneity, reflecting a wider range of adsorption site energies on the material (Marliza et al. 2017). The data in Table 2 shows the Freundlich isotherm constants for the fitting models of CO_2 adsorption for Zn-porphyrin **5**.

Based on the low K_f value shown in Table 2, the adsorption capacity under the studied conditions is considered modest. However, this result remains meaningful, as the corresponding 1/*n* value indicates the presence of a heterogeneous surface, while suggesting a strong interaction between the adsorbent and CO_2 molecules.

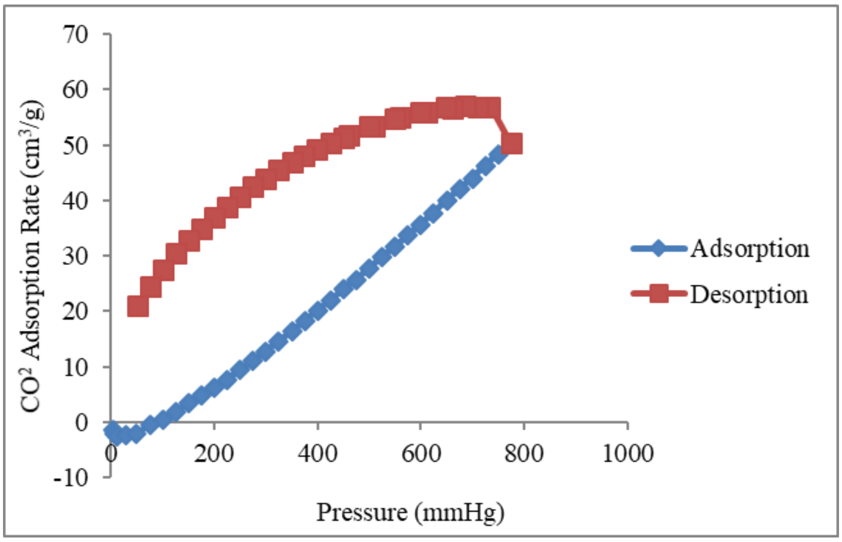

FIGURE 8. Adsorption and desorption isotherm of porphyrin **5** at temperature of 25 °C

TABLE 2. Freundlich isotherm constant of fitting model for CO_2 adsorption on Zn (II) porphyrin 5

	Freundlich constant		Correlation coefficient (R^2)
	K_f(mg/g)	1/*n*	
Zn-porphyrin 5	0.00151	0.595	0.984

CONCLUSION

Overall, 5,15-A_2 porphyrin and metalloporphyrin have been successfully synthesized with satisfactory yields. Characterization by ^{1}H NMR spectroscopy clearly showed a signal in the negative chemical shift region, which confirms the successful formation of the free-base porphyrin, attributed to the presence of NH protons located at the center of the macrocyclic ring. In the case of metalloporphyrins, successful formation is confirmed by the disappearance of the negative chemical shift signal in the ^{1}H NMR spectrum, indicating the replacement of the central NH protons by the metal ion within the porphyrin core. Additionally, characterization via UV-Vis spectroscopy is crucial, as the spectrum provides clear evidence of porphyrin formation. For free-base porphyrins, the spectrum typically exhibits one intense Soret band and four Q bands, while for metalloporphyrins, it shows one Soret band along with only two Q bands. This reduction in the number of Q bands upon metallation reflects the increase in molecular symmetry and the elimination of NH-associated electronic effects in the macrocyclic core. Based on the preliminary evaluation of carbon dioxide adsorption data, the high correlation coefficient (R^2) obtained from the Freundlich isotherm model of Zn (II) porphyrin 5 indicates that the CO_2 adsorption pattern is better described by this model compared to the Langmuir isotherm, which did not exhibit a good linear correlation. Additionally, it can be concluded that metalloporphyrins, particularly Zn (II) porphyrins with hexyl functional group exhibit the highest CO_2 uptake among the synthesized porphyrins, and a promising candidate among porphyrin derivatives for application in carbon dioxide adsorption and capture systems. While Cu (II) porphyrins have been extensively studied and widely incorporated into hybrid materials such as metal–organic frameworks (MOFs), the results suggest that Zn (II) porphyrins also represent a viable and underexplored alternative, warranting further investigation for similar integration and application. Nevertheless, there are still numerous possibilities for porphyrins modifications in order to improve and increase the carbon dioxide adsorption ability, hence further enhancing the potential of porphyrin compounds. These include the incorporation of long alkyl chains like octyl. This flexible side chain prevents dense packing, promotes looser molecular arrangement, and creates free volume and micropores that facilitate CO_2 adsorption. Additionally, the introduction of polar groups can be explored to enhance the weak interaction and the disruption of π–π stacking to maximize surface accessibility. In terms of analysis, as this study represents a preliminary evaluation of the CO_2 adsorption capacity of porphyrin compounds, it does not include surface area and pore size distribution measurements, which are essential for gaining deeper insight into the relationship between material porosity and CO_2 uptake. Future work should consider incorporating surface characterization techniques such as the BET (Brunauer–Emmett–Teller) method for surface area determination and the BJH (Barrett–Joyner–Halenda) method for pore size distribution to better understand the textural properties and adsorption behavior of the porphyrin materials.

EXPERIMENTAL SECTION

The main chemicals used in the synthesis of all compounds were pyrrole 98% (Sigma Aldrich), benzaldehyde (R&M), heptanal (R&M), trifluoroacetic acid 99% (Sigma Aldrich), 2,3-dichloro-5,6-dicyano-1,4-benzoquinone (DDQ) (Sigma Aldrich) and triethylamine (TEA), used without further purification. Nuclear magnetic resonance spectroscopy (NMR) proton (^{1}H-NMR) and carbon (^{13}C-NMR) spectrums were recorded on a Bruker 400 MHz in deuterated chloroform ($CDCl_3$). UV-Vis spectra were recorded using UV-1800 Shimadzu Spectrophotometer at wavelength of 350-700 nm and dichloromethane (DCM) as the solvent.

SYNTHESIS OF PORPHYRIN

The experimental procedure for dipyrromethane **1** was comprehensively documented by Radzuan et al. (2021, 2018). Yield 6 g (38%) as pale-yellow solid; ^{1}H NMR (400 MHz, $CDCl_3$) δ 7.70 (s, 2H), 6.64 (dd, *J* = 1.60 Hz, 2H) 6.21 (dd, *J* = 2.80 Hz, 2H), 6.10 (dd, 2H), 3.96 ppm (s, 2H) ppm. The NMR data were in accordance with the literature (Basic 2010; Groves et al. 2013).

SYNTHESIS OF 5,15-A_2 PORPHYRIN

The experimental procedures for 5,15-A_2 porphyrin **2** and 3 were comprehensively documented by Radzuan et al. (2021, 2018).

Porphyrin **2**: Dipyrromethane (1.0 g, 6.80 mmol) **1** reacted with benzaldehyde (0.7 mL, 6.80 mmol) to yield porphyrin 2 as dark purple crystal. Molecular formula: $C_{32}H_{22}N_4$; Yield: 500 mg (30%); melting point: > 300 °C; R_f 0.44 (hexane/DCM, 3:2 v/v); ^{1}H NMR (400 MHz, $CDCl_3$) δ -3.09 (s, 2H), 7.85 (m, 6H), 8.31 (m, 4H), 9.13 (d, *J*=4.40 Hz, 4H), 9.43 (d, *J*=4.40 Hz, 4H), 10.34 (s, 2H) ppm. ^{13}C NMR (100.6 MHz, $CDCl_3$) δ 147.2, 145.2, 141.4, 134.9, 131.7, 131.1, 127.8, 127.0, 119.1, 105.3 ppm; UV-Vis (CH_2Cl_2): λ_{max} nm (log ε) = 403.6 (5.70), 505.2 (4.62), 540.8 (4.35), 575.6 (4.38), 631.2 (4.28). ESI-SJ (m/z) literature: 462.18 [M^+]. The NMR data were in agreement with the literature (Xin et al. 2014).

Porphyrin **3**: Dipyrromethane (1.0 g, 6.80 mmol) **1** reacted with heptaldehyde (0.8 mL, 6.80 mmol) to yield porphyrin **3** as dark purple crystal. Molecular formula: $C_{32}H_{38}N_4$; Yield: 370 mg (23%); melting point: 240 - 250 °C; R_f 0.5 (hexane: DCM, 1:1); ^{1}H NMR (400 MHz, $CDCl_3$) δ -2.95 (s, 2H), 0.97 (t, JHH = 7.2 Hz, 6H), 1.43 (m, 4H), 1.56 (m, 4H), 1.84 (m, 4H), 2.57 (m, 4H), 5.00 (t, JHH = 8.0 Hz, 4H), 9.41 (d, 3JHH = 4.4 Hz, 2H), 9.58 (d, 3JHH = 4.4 Hz, 4H), 10.17 (s, 2H) ppm. ^{13}C NMR

(100.6 MHz, $CDCl_3$) δ 14.2, 22.8, 30.3, 31.9, 34.7, 38.7, 104.3, 118.8, 127.8, 131.9, 144.2, 147.8 ppm; UV-Vis (CH_2Cl_2): λ_{max} nm (log ε) = 403 (5.36), 501 (4.26), 534 (4.02), 577 (4.03), 629 (3.92); ESI-SJ (m/z) literature: 478.31 $[M]^+$. The NMR data were in agreement with the literature (Ryppa et al. 2005).

METALLATION OF PORPHYRIN WITH ZINC

Porphyrin was dissolved in chloroform ($CHCl_3$) (10 mL) and heated to reflux for 10 to 15 min. Zinc (II) acetate was dissolved in methanol (MeOH) and subsequently added to the porphyrin solution. The reaction mixture was then refluxed for an additional 15 to 30 min, with progress monitored using thin-layer chromatography (TLC). After completion, all solvents were removed via rotary evaporation, and the residue was purified by column chromatography using chloroform as the eluent. The purified compound was further recrystallized with dichloromethane/methanol dual-solvent system to obtain the zinc porphyrin complex.

Porphyrin **4**: Porphyrin **2** (50 mg, 0.1 mmol) reacted with Zn $(OAc)_2$ (50 mg, 0.28 mmol) to yield porphyrin **4** as reddish purple solid. Molecular formula: $C_{32}H_{20}N_4Zn$; Yield: 56 mg (99%); melting point: 360 °C; R_f 0.6 (hexane: chloroform, 1:1); ^1H NMR (400 MHz, $CDCl_3$) δ 7.83 (m, 6H), 8.30 (dd, $^3J_{HH}$ = 6.8 Hz, $^4J_{HH}$ = 1.6 Hz, 4H), 9.18 (d, $^3J_{HH}$ = 4.4 Hz, 4H), 9.48 (d, $^3J_{HH}$ = 4.40 Hz, 4H), 10.37 (s, 2H) ppm. UV-Vis (CH_2Cl_2): λ_{max} nm (log ε) = 407 (5.27), 532 (3.79). ESI-SJ (m/z) literature: 524 $[M]^+$ (Senge et al. 2015). The NMR data were in agreement with the literature (Senge et al. 2015).

Porphyrin **5**: Porphyrin **3** (50 mg, 0.1 mmol) reacted with Zn $(OAc)_2$ (50 mg, 0.28 mmol) to yield porphyrin **5** as reddish-purple solid. Molecular formula: $C_{32}H_{36}N_4Zn$; Yield: 50 mg (88%); melting point: 350 °C; R_f 0.5 (chloroform); ^1H NMR (400 MHz, $CDCl_3$) δ .98 (t, J_{HH} = 6.2 Hz, 6H), 1.27 (m, 4H), 1.46 (m, 4H), 1.87 (m, 4H), 2.61 (m, 4H), 5.07 (t, J_{HH} = 7.2 Hz, 4H), 9.45 (d, $^3J_{HH}$ = 2.0 Hz, 4H), 9.69 (d, $^3J_{HH}$ = 2.0 Hz, 4H), 10.14 (s, 2H) ppm; UV-Vis (CH_2Cl_2): λ_{max} nm (log ε) = 406 (5.25), 536 (3.80); ESI-SJ (m/z) literature: 540.22 $[M]^+$ (Senge et al. 2015). The NMR data were in agreement with the literature (Senge et al. 2015).

METALLATION OF PORPHYRIN WITH NICKEL

Porphyrin and nickel (II) acetylacetonate were dissolved in toluene and heated to reflux, with the reaction progress monitored using thin-layer chromatography (TLC). After completion, toluene was removed via rotary evaporation, and the residue was purified by column chromatography using a hexane-chloroform solvent system. The purified compound was further recrystallized with chloroform/hexane dual-solvent system in order to yield the nickel porphyrin complex.

Porphyrin **6**: Porphyrin **2** (50 mg, 0.1 mmol) reacted with $Ni(acac)_2$ (300 mg, 1.2 mmol) to yield porphyrin **6** as reddish-purple crystal. Molecular formula: $C_{32}H_{40}N_4Ni$; Yield: 15 mg (30%); melting point: 366 °C; R_f 0.7 (hexane: chloroform, 2:1); ^1H NMR (400 MHz, $CDCl_3$) δ 7.76 (m, 6H), 8.10 (d, $^3J_{HH}$ = 5.2 Hz), 8.96 (d, $^3J_{HH}$ = 4 Hz, 4H), 9.22 (d, $^3J_{HH}$ = 4.4 Hz, 4H), 9.97 (s, 2H) ppm; UV-Vis (CH_2Cl_2): λ_{max} nm (log ε) = 399 (5.13), 511 (3.94), 546 (3.65); ESI-SJ (m/z) literature: 518 $[M]^+$ (Senge et al. 2015). Characterization data obtained were in agreement with the literature (Senge et al. 2015).

Porphyrin **7**: Porphyrin **3** (50 mg, 0.1 mmol) reacted with $Ni(acac)_2$ (350 mg, 1.2 mmol) to yield porphyrin **7** as reddish-purple crystal. Molecular formula: $C_{32}H_{36}N_4Ni$; Yield: 46 mg (82%); melting point: 384 °C; R_f 0.5 (hexane: chloroform, 2:1); ^1H NMR (400 MHz, $CDCl_3$) δ 0.93 (t, J_{HH} = 7.2 Hz, 6H), 1.38 (m, 4H), 1.47 (m, 4H), 1.68 (m, 4H), 2.39 (m, 4H), 4.70 (t, J_{HH} = 8.2 Hz, 4H), 9.20 (d, $^3J_{HH}$ = 4.8 Hz, 4H), 9.47 (d, $^3J_{HH}$ = 4.8 Hz, 4H), 9.74 (s, 2H) ppm; UV-Vis (CH_2Cl_2): λ_{max} nm (log ε) = 400 (5.25), 515 (4.04), 549 (3.57); ESI-SJ (m/z) literature: 534.23 $[M]^+$ (Senge et al. 2015). Characterization data obtained were in agreement with the literature (Senge et al. 2015).

PHYSICAL CO_2 ADSORPTION-DESORPTION MEASUREMENT

The Micromeritics ASAP 2020 gas adsorption analyzer was used to study the physical adsorption-desorption of CO_2, following the procedure reported by Marliza et al. (2017). Approximately 0.3 g of the sample was placed in a sample tube and was degassed at 150 °C to remove any adsorbed moisture, impurities, or surface contaminants. After a 10-h degassing process, the sample was transferred from the degassing port to the analysis port for CO_2 adsorption evaluation at 1 atm and 25 °C with circulated water bath, using 98% purified CO_2 gas as an adsorbate. The adsorption-desorption data were subsequently analyzed using the ASAP 2020 operating software.

ACKNOWLEDGEMENTS

We would like to express our sincere gratitude to Universiti Kebangsaan Malaysia for providing the research facilities. Special thanks to Ministry of Science and Technology Innovation (Grant FRGS/1/2014/SG01/UKM/02/5) and Ministry of Higher Education Malaysia (MybrainSc scholarship) for their financial supports.

REFERENCES

Basic, B. 2010. Azo- and butadiyne-linked 5,10-diarylporphyrins. Ph.D. Thesis, Science and Technology, Queensland University of Technology (Unpublished).

Creamer, A.E. & Gao, B. 2015. *Carbon Dioxide Capture: An Effective Way to Combat Global Warming*. London: Springer.

Ghazali, Z., Yarmo, M.A., Hassan, N.H., Teh, L.P. & Othaman, R. 2020. New green adsorbent for capturing carbon dioxide by choline chloride: Urea-confined nanoporous silica. *Arabian Journal for Science and Engineering* 45: 4621-4634.

Giovannetti, R. 2012. The use of spectrophotometry UV-Vis for the study of porphyrins. *Macro to Nano Spectroscopy,* edited by Uddin, J. InTech. Doi: 10.5772/2503

Groves, B.R., Crawford, S.M., Lundrigan, T., Matta, C.F., Hashjin, S.S. & Thompson, A. 2013. Synthesis and characterisation of the unsubstitued dipyrrin and 4,4-dichloro-4-bora-3a, 4a-diaza-*s*-indacene: Improved synthesis and functionalization of the simplest bodipy framework. *Chemical Communications* 49: 816-818.

International Energy Agency. 2023. CO_2 emission in 2023. *IEA Publications*. Available at CO_2 Emissions in 2023 - Analysis - IEA (Accessed on 24 March 2025).

International Energy Agency. 2022. CO_2 emission in 2022. *IEA Publications*. Available at CO_2 Emissions in 2022 - Analysis - IEA (Accessed on 24 March 2025).

Kumar, S., Mohmmad, Y.W., Arranja, C.T., Silva, J.D.A., Avula, B. & Sobral, A.J.F.N. 2015. Porphyrins as nanoreactors in the carbon dioxide capture and conversion: A review. *Journal of Material Chemistry A* 3: 19615-19637.

Laha, J.K., Dhanalekshmi, S., Taniguchi, M., Ambroise, A. & Lindsey, J.S. 2003. A scalable synthesis of meso- substituted dipyrromethanes. *American Chemical Society* 7(6): 799-812.

Liu, Y., Yang, Y., Sun, Q., Wang, Z., Huang, B., Dai, Y. & Qin, X. 2013. Chemical adsorption enhanced CO_2 capture and photoreduction over a copper porphyrin-based metal organic framework. *American Chemical Society Applied Materials & Interfaces* 5(15): 7564-7568.

Locos, O.B. 2006. Synthesis and investigations of novel alkenylporpyhyrins and bis (porphyrins). Ph.D. Thesis, Faculty of Science and Technology, Queensland University of Technology (Unpublished).

Marliza, T.S., Yarmo, M.A., Hakim, A., Tahari, M.N.A., Hisham, M.M.H. & Yap, Y.H.T. 2017. CO_2 capture on NiO supported imidazolium- based ionic liquid. *AIP Conference Proceedings* 1838: 020008.

Pereira, N.A.M. & Pinho, T.M.V.D. 2014. Recent development in the synthesis of dipyrromethane. A review. *The New Journal of Organic Synthesis* 46(3): 183-213.

Radzuan, N.H.M., Malek, N.H.A., Ngatiman, M.F., Xin, T.K., Bakar, M.B., Hassan, N.I. & Bakar, M.A. 2018. Synthesis and x-ray single crystal study of 5-(4,4,5,5-tetramethyl-1,3,2-dioxoborolane)-10-20-diphenylporphyrin. *Sains Malaysiana* 47(9): 2083-1090.

Radzuan, N.H.M., Norazmi, N.A.Z., Ali, A.H., Bakar, M.A., Agustar, H.K., Razak, M.R.M. & Hassan, N.I. 2021. Synthesis, *in-vitro* antiplasmodial activity and cytotoxicity of metalloporphyrins against *Plasmodium falciparum* K1 strain. *Sains Malaysiana* 50(10): 2945-2956.

Rajasree, S.S., Li, X. & Deria, P. 2021. Physical properties of porphyrin-based crystalline metal-organic frameworks. *Communications Chemistry* 4: 47.

Ryppa, C., Senge, M.O., Hatscher, S.S., Kleinpeter, E., Wacker, P., Schilde, U. & Wiehe, A. 2005. Synthesis of mono- and disubstituted porphyrins: A- and 5,10-A_2 type systems. *Chemical European Journal* 11: 3427-3442.

Senge, M.O., Flanagan, K.J., Ryan, A.A., Ryppa, C., Donath, M. & Twamley, B. 2015. Conformational and structural studies of *meso* monosubstituted metalloporphyrin – edge-on molecular interactions of porphyrins in crystal. *Tetrahedron* 72(1): 105-115.

Shanmugathasan, S., Edwards, C. & Boyle, R.W. 2000. Advances in modern synthetic porphyrin chemistry. *Tetrahedron* 56: 1025-1046.

Shi, Y., Zhang, F. & Linhardt, R.J. 2021. Porphyrin-based compounds and their application in materials and medicine. *Dyes and Pigments* 188: 109136.

Wamser, C.C. & Ghosh, A. 2022. The hyperporphyrin concept: A contemporary perspective. *American Chemical Society* 2: 1543-1560.

Xin, T.K., Lintang, H.O., Tamuri, A.R., Endud, S. & Bakar, M.B. 2014. Synthesis and emission properties of meso-substituted porphyrins. *Jurnal Teknologi* 71(1): 19-25.

*Corresponding author; email: muntaz@ukm.edu.my

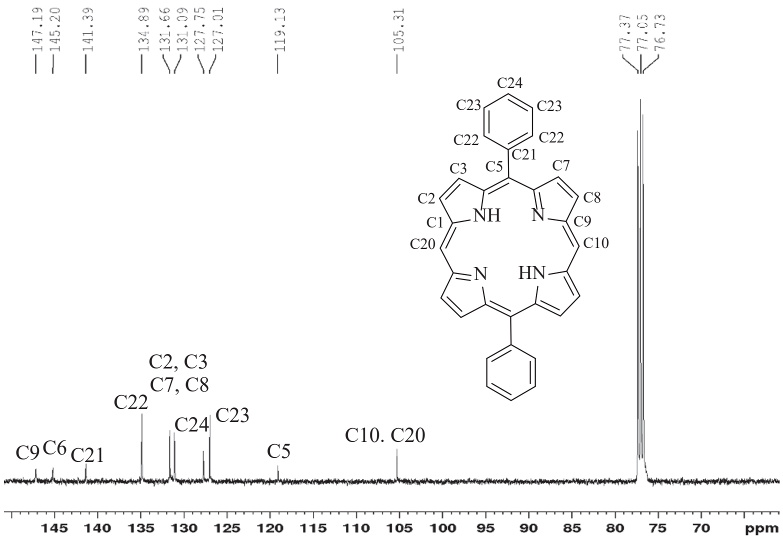

FIGURE S1. ^{13}C-NMR of porphyrin **2** in $CDCl_3$ at room temperature

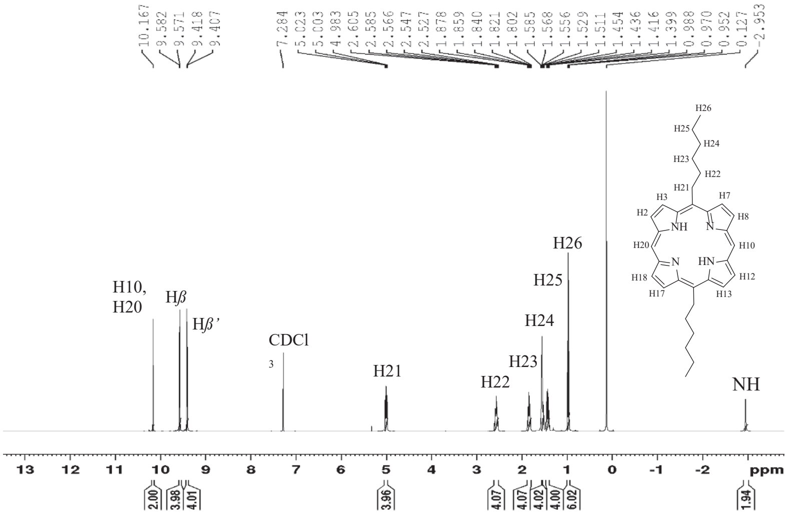

FIGURE S2. ^{1}H-NMR of porphyrin **3** in $CDCl_3$ at room temperature

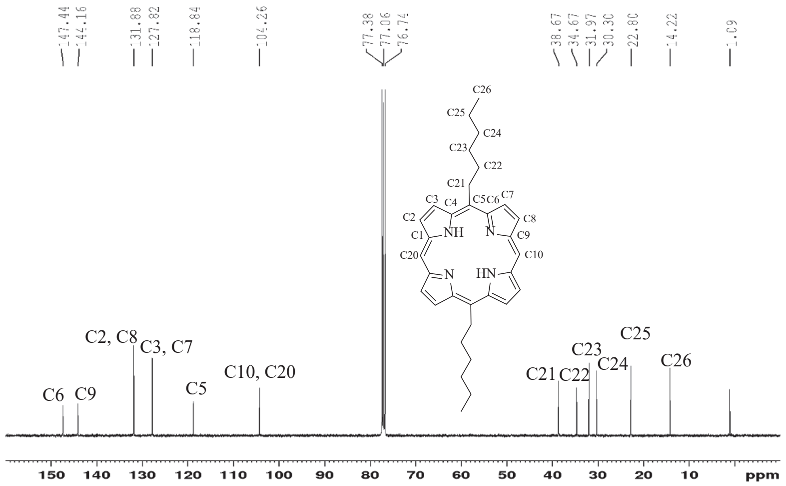

FIGURE S3. ^{13}C-NMR of porphyrin **3** in $CDCl_3$ at room temperature

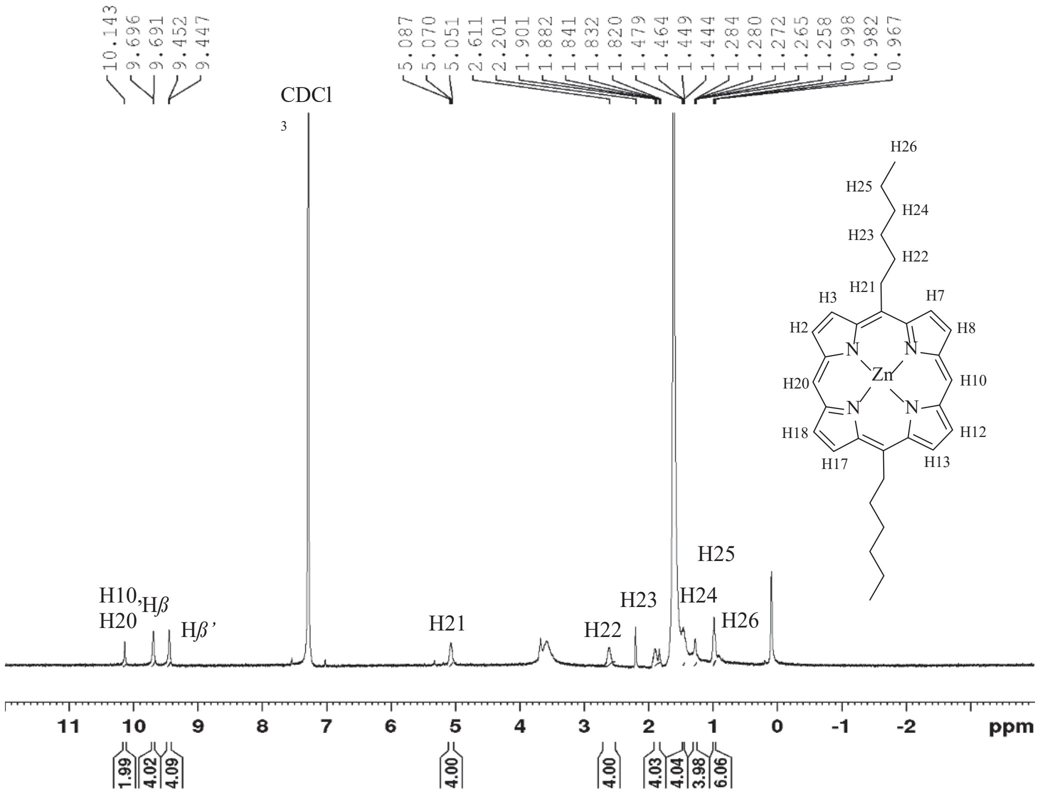

FIGURE S4. ^{1}H-NMR of Zn (II) porphyrin **5** in CDCl$_3$ at room temperature

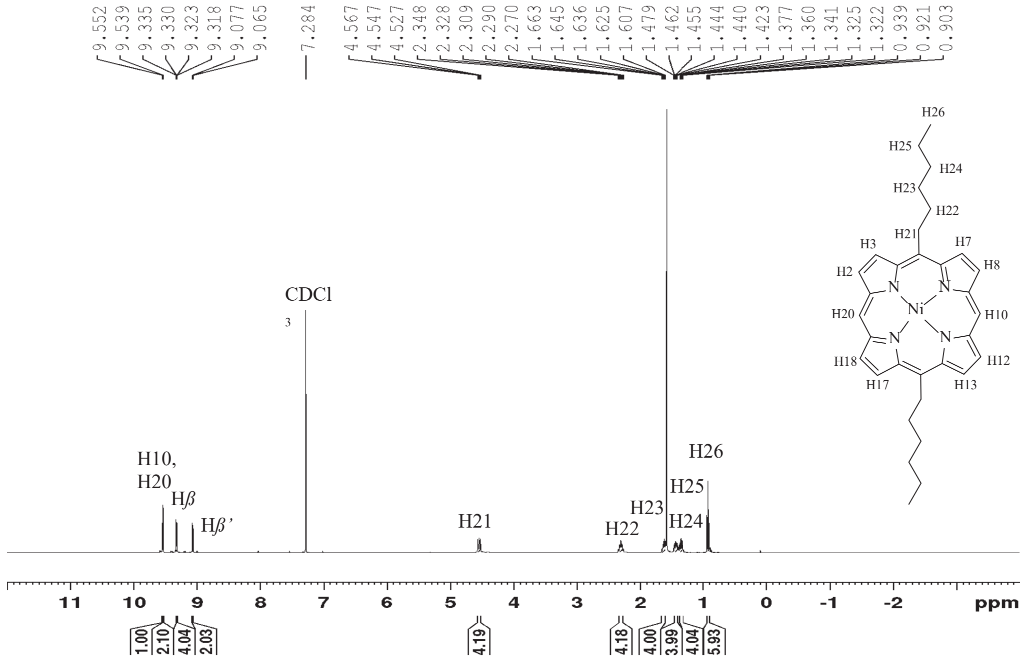

FIGURE S5. ^{1}H-NMR of Ni (II) porphyrin **7** in CDCl$_3$ at room temperature

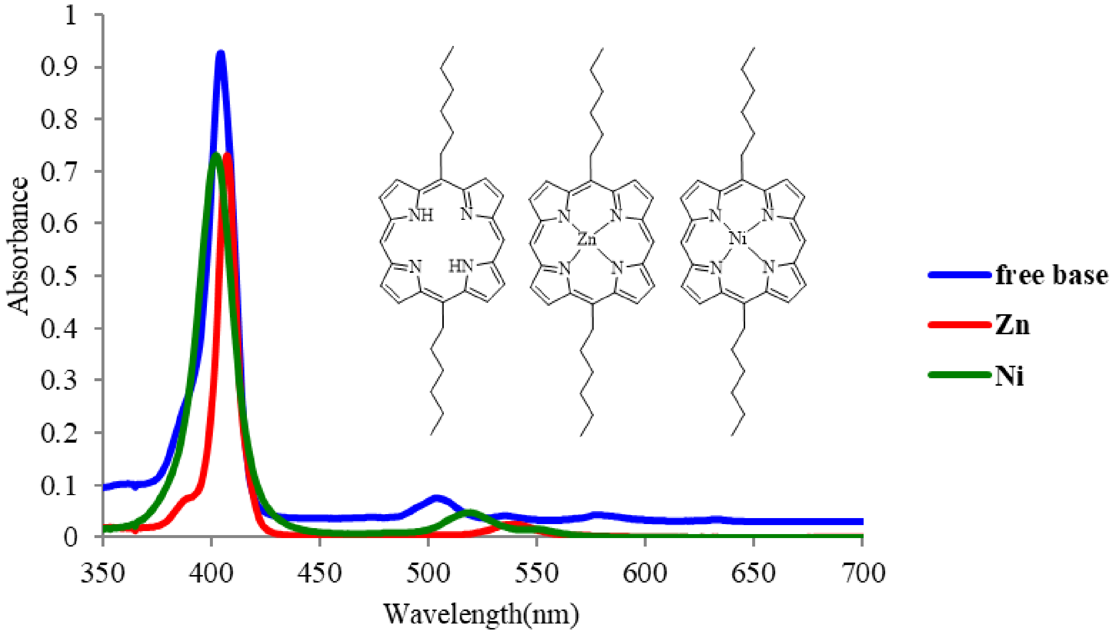

FIGURE S6. UV-Visible spectrum of free-base porphyrin **3** and metalloporphyrin **5** and **7** at concentration of 4.0 × 10^{-6} M in dichloromethane ($CHCl_2$) at room temperature

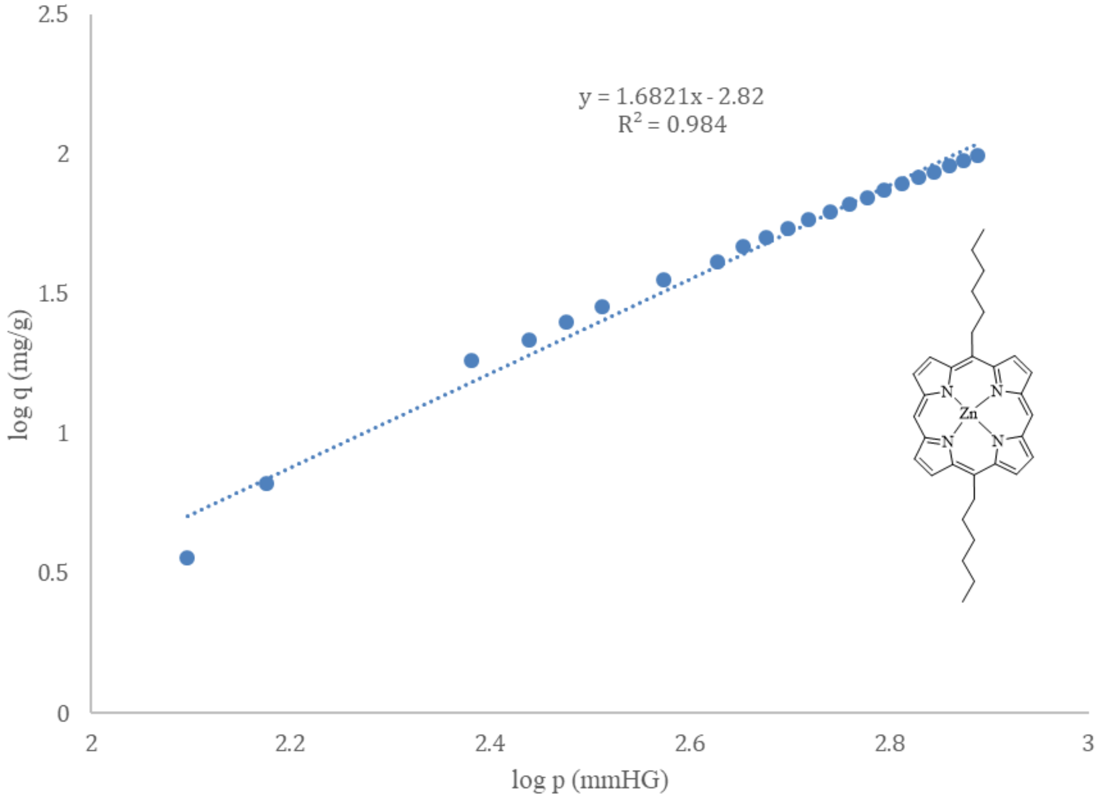

FIGURE S7. Freundlich isotherm constant of fitting model for CO_2 adsorption on Zn (II) porphyrin **5**